MAXIMUM CURRENT LIMITATIONS AND TRANSPORT PROCESSES IN THE ELECTRODE OF THE PEM FUEL CELL

K. ZHUKOVSKY, A. POZIO

ENEA - Grande Progetto Idrogeno e Celle a Combustibile
Centro Ricerche Casaccia, Roma

RT/2003/59/IDROCOMB

ENTE PER LE NUOVE TECNOLOGIE,
L'ENERGIA E L'AMBIENTE

MAXIMUM CURRENT LIMITATIONS AND TRANSPORT PROCESSES IN THE ELECTRODE OF THE PEM FUEL CELL

K. ZHUKOVSKY, A. POZIO

ENEA - Grande Progetto Idrogeno e Celle a Combustibile
Centro Ricerche Casaccia, Roma

RT/2003/59/IDROCOMB

MAXIMUM CURRENT LIMITATIONS AND TRANSPORT PROCESSES IN THE ELECTRODE OF THE PEM FUEL CELL

K. ZHUKOVSKY, A. POZIO

Abstract
Performance of PEFC in the regime of limiting current is modelled. Maximum current limitations, due to the oxygen deplete on the cathode side are considered. The effect of the geometry of the gas diffuser and supply channels, geometric and physical characteristics of the diffuser and the pressure regime of the PEFC is investigated. Effect of liquid water in the electrode and air pressure in gas channels is studied to identify the best geometry of the gas supply net in the terms of the maximum cell current. Comparison between model predictions and experimental data is carried out.

Key words: model, limiting oxygen flux, water, diffuser, serpentine gas channel and pressure.

MODELLO DELLE PRESTAZIONI E DEI PROCESSI DI TRANSPORTO ELETTRODICI DI PEFC IN CONDIZIONI DI CORRENTE LIMITE

Riassunto
E' stato realizzato un modello delle prestazioni di una PEFC in condizioni di funzionamento di corrente limite. Sono state considerate le limitazioni di corrente massima dovute al consumo di ossigeno dal lato catodo. Sono state indagate in particolare, gli effetti della geometria dei canali in cui scorre il gas di alimentazione, le caratteristiche geometriche e fisiche di tali diffusori in condizioni di regime di pressione della PEFC. Sono stati analizzati gli effetti dell'acqua liquida all'interno degli elettrodi e della pressione dell'aria nei canali per identificare la migliore geometria possibile di alimentazione del gas in termini di corrente massima di cella. Sono stati effettuati paragoni tra dati sperimentali e dati calcolati mediante il modello.

Parole chiavi: modello, corrente limite, ossigeno, acqua liquida, diffusori, alimentazione del gas e pressione.

Introduction

Polymer electrolyte fuel cells (PEFC) represent increasingly popular alternative sources of energy. However, fuel cells with high power densities must be developed for this technology to become a viable power source for transportation applications. Three main factors, limiting the current and leading to voltage losses in proton conducting membrane fuel cells are the following: activation resistance, attributed to the catalyst layer in contact with electrode and accessible by reacting gases [1-4], ohmic voltage losses, attributed to the electronic, ionic and contact resistance of the cell [5-9] and the mass transport resistance, when the reactant gases deplete on the reaction interface as their transport to the reaction sites fails to keep up with the reaction rate. During the operation, reactant gases flow down the channels, diffusing into the electrodes through the diffusion layers to the catalyst interfaces. At high current densities, the reaction rate becomes mass-transfer limited by the transport of the reactant gases from the channel to the catalyst surface. The last phenomenon, present in particular on the cathode, still has not been fully addressed by researchers. The only common method to overcome such transport limitations and to increase the power density has been to use pressured reactants.

So far, numerous theoretical models of PEFC have been developed (see, for example, [10-17]). However, they are usually restricted to simple one-dimensional cases. Recent experimental studies demonstrated significant influence of final pressure drops and geometry of supply channels on the effectiveness of the cell [18-21]. For example, interdigitated and serpentine configurations of supply channels essentially make use of a new pressure driven mechanism of mass transport that acts additionally to common molecular diffusion.

In the present study we restrict our attention to the oxygen electrode, which has been the subject of numerous studies and which is the limiting electrode, compared to the relatively efficient hydrogen electrode of PEFC. At the cathode, the reaction rate is limited by the transport of oxygen from the channels to the catalyst sides and of the water vapour in the opposite direction. In addition to the gas transport limitations the cathode faces another problem, called electrode flooding. The water generation rate at the cathode at high current densities often exceeds its removal rate from the inner porous layers in the form of water vapour, resulting in condensation.

When the gases are forced to flow into the diffuser from the gas channels, adding convection mechanism of mass transport to pure diffusion. Since convection is much faster than diffusion, the reaction rates at the catalyst can be significantly improved. Furthermore, the shear force of this gas flow field helps remove most of the liquid water that is entrapped into the inner layers of the electrode, reducing the flooding problem. This effect is present not only in so called interdigitated channels with closed ends where gas is forced to flow through the electrode to exit, but also some other geometric configurations, such as

serpentine channels. However, the air meets high flow resistance in interdigitated flow and it results in low airflow rates, low outlet oxygen concentration. On the contrary, serpentine design makes use of both advantages of the conventional and interdigitated flow fields. When serpentine channels in the electrode are set under pressure, the flow rate of air along the channels becomes sufficiently high, providing enough oxygen supply for the device, whereas oxygen is transported to the inner layers of the electrode by both diffusion and convection that is induced by the pressure drop between the neighbouring channels.

We first report the experimental part, then we describe the 2-dimensional electrode model mathematically and apply the model for the comparative analysis of the maximum current limitations of the PEFC, running it along the 3d dimension for specific configurations of gas supply channels of serpentine design. In particular, the nets of 2, 3, 4, 5, 7 and 10 parallel serpentine channels on a square plate will be considered. The aim of the studies is the identification of most efficient in the terms of the limiting current, channel configuration. Then, the model results are analysed and compared with experimental results.

Experimental

Materials

Commercially available 20 wt% Pt/C catalyst powders on carbon black (Vulcan XC72) were purchased from E-Tek Inc. Three-layer (substrate/diffusive layer/catalyst layer) gas diffusion anode and cathode (106 cm^2) were prepared using a spray technique described in detail in previous works [22-24]. The substrate was carbon paper (Toray TGPH090). The weight composition of the diffusion layer was 85 wt.% of carbon and 15 wt.% of PTFE, with carbon loading of 1.93 mg cm^{-2}. The catalyst layer was prepared by mixing appropriate amounts of carbon-supported catalyst (24.5 wt.%) and 5 wt.% Nafion ionomer solution from Aldrich (14.9 wt.%) and glycerol (60.5 wt.%). The platinum loading in all anodes and cathodes was kept constant at 0.34 mg cm^{-2} on the MEA. Nafion 115 membrane (Du Pont) was used after purification treatment in 5 w/v.% H_2O_2 solution at 80°C for 1 h, followed by a second treatment in 1 M H_2SO_4. The MEAs were formed by hot pressing the electrodes (106 cm^2) onto the membrane at 130°C for 1-5 minutes and 50-100 kg cm^{-2}.

Membrane electrode gasket assembly (MEGA) technology [22] was used and a well-defined shape compatible with the cell hardware was achieved (Fig. 1).

This technology allows to disassemble the cell and to replace the graphite plates, maintaining the same MEA [22]. In this work, aluminium anticorrodal 100 (Alusuisse) end plates (185 mm x 185 mm x 11 mm) were used. At the lateral borders of the assembly and end plates, manifolds holes for gas feeding are visible (Fig. 1). Graphite flow field plates were assembled with a typical parallel channel configuration (three or ten channels on the cathode side and ten channels on the anode side) using commercially available BMA5 graphite produced by SGL Carbon Group (Germany).

Electrochemical characterisation

Full-cell electrochemical tests were carried out in the ten or three channels systems using a 106 cm^2 single cell incorporated in a Globe Tech Inc mod. 890 test station. Two aluminium end plates and two graphite current collectors composed the single cell. The MEGA system and the other components of single fuel cell are schematised in Fig.1:

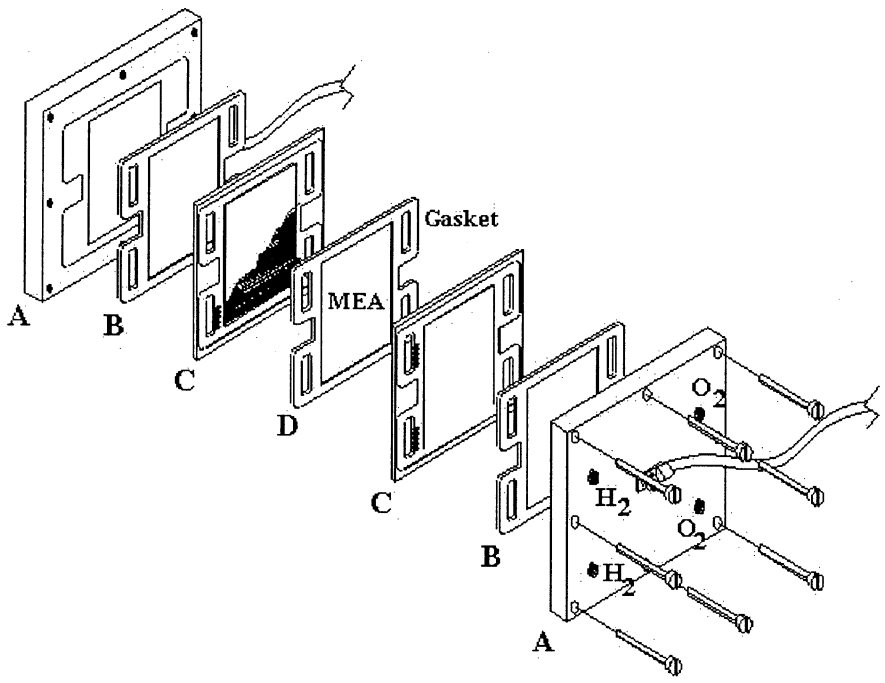

Figure 1. *Schematic of a single PEM fuel cell showing the location of the components: A) aluminium or SS316L end plates, B) copper current collector/gaskets, C) graphite flow field plates, D) MEGA*

Cell voltage vs. current density measurements were galvanostatically performed with a programmable power supply interfaced with a computer for data acquisition. The results are given on the Fig.2:

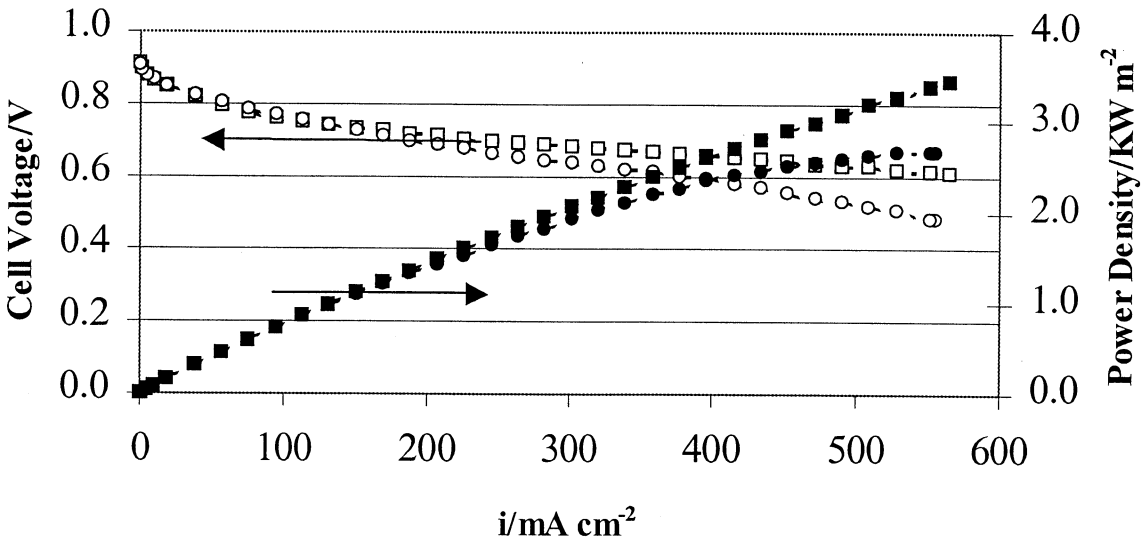

Figure 2. *Cell voltage and power density vs. current density for 3 (squares) and 10 (circles) cathode channels configuration, at T_{cell}=75°C under H_2 14 scc/min/A and O_2 52.5 scc/min/A flux at 1.5/1.5 abs bar.*

All measurements were carried at 75°C in H_2/O_2 flux at 1.5/1.5 bar absolute pressure. The temperature humidifier was kept at 85°C for the anode and 50°C for the cathode.

Description of the model

A porous electrode is a very complicated structure, which is difficult to characterise on a microscopic level. One approach to this problem is a porous electrode theory [25]. It employs the macroscopic model that accounts for the essential features of a porous electrode without going deep into exact details. The development of the equations for describing the membrane oxygen transport in the gas diffuser in this model is based on such macrohomogenious description with uniform morphological properties such as porosity, tortuosity, and permeability.

In order to analyse the diffusion effects on cathode behaviour and address current limitations, we assumed a simplified approximation of isothermal properties for system, and the gas mixture is considered a perfect gas. In actual fuel cells and especially in multi-cell stacks, thermal gradients are likely to apply due to the heats of reaction on the electrodes and the product water is likely to be a mixture of liquid and vapour. However, with the available apparatus it is hardly possible to characterise these gradients and state

of water precisely. Moreover, the temperature gradient in the cathode effects density and diffusivity coefficients, but the density diffusivity product that characterises the oxygen transport varies less than 4% for practical temperatures in PEFC if the entering the channel air is fully saturated [18].

In the pores of the gas diffuser, we assume that the water vapour is equilibrated with liquid water in the form of small water drops. Though different approaches have been adopted by different researches [26, 27], in the present work we assume that liquid water does not constitute a continuous barrier to oxygen transport [28].

Water leaves the channels and enters the electrode in the form of saturated water vapour only.

We also assume that the water in the gas diffuser takes off only a negligible amount of dissolved oxygen and nitrogen, compared to the large gas phase.

The active catalyst layer is assumed to exist only as an ultra thin plane, so that the transport of the reactants within this layer can be neglected.

We also assume the steady state processes, absence of sinks and sources in the body of the diffuser and the electrochemical reaction takes place on the surface of the catalyst layer only. Other assumptions will be discussed as the model equations are presented. The schematic drawing of the electrode of the polymer electrolyte fuel cell is given on the Fig. 3:

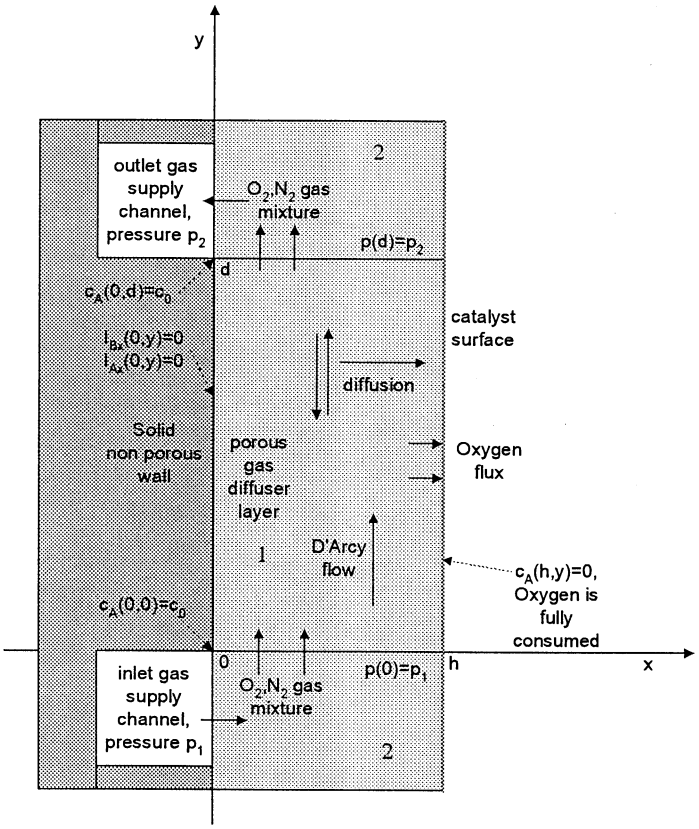

Figure 3. *Schematic drawing of an electrode of a polymer electrolyte fuel cell.*

Then, the fluxes of gases in the body of the electrode are governed by well-known equations of diffusion, continuity equations and D'Arcy flow equation [29]:

$$\vec{I}_i = -\rho D_i \vec{\nabla} c_A + g\rho_i \vec{u}, \quad \vec{\nabla}\vec{I}_i = 0, \quad \vec{u} = -\frac{k}{\mu}\vec{\nabla} p,$$
$$\sum_i c_i = 1, \; c_i = \rho_i / \rho, \; p = \rho RT, \tag{1}$$

where $\vec{I}_i$, are the fluxes of i substances, c_i are their concentrations, ρ_i are their densities, ρ is total density, p – pressure, D_i – diffusion coefficients of gases into the mixture, $\vec{u}$ – bulk speed of the gas mixture, R – gas constant, T – temperature, k – permeability coefficient, μ – viscosity coefficient.

Usually, gas pressures are approximately equal to each other at the anode and the cathode of PEFC. Then the assumption $p = p(y), p(x) = const$ is justified. In order to address oxygen transport limitations, oxygen of initial concentration c_0 is considered to be fully converted on the catalyst surface of PEFC. Boundary conditions in such case of limiting current read as follows (see Fig. 3):

$$p(0) = p_1, p(d) = p_2, c_{O2}(h, y) = 0, c_{O2}(0,0) = c_0, c_{O2}(0, d) = c_1, I_{i,x}(x = 0, y) = 0. \tag{2}$$

Diffusion coefficient D_i is a function of temperature, pressure and gas composition. The effective oxygen diffusion coefficient in nitrogen – water vapour mixture can be calculated as a function of binary diffusion coefficients:

$$D_{O2} = \frac{1 - (c_{O2} M_{O2} / M)}{\frac{c_w}{D_{O2-w}} + \frac{c_{N2}}{D_{O2-N2}}}, \; c_w = \frac{p_w^{sat}}{p}, \; \sum_i c_i M_i = M, \tag{3}$$

where , c_w is the concentration of water vapour, c_{O2} is the concentration of oxygen, $D_{O2\text{-}w}$ – diffusion coefficients of oxygen in water vapour, $D_{O2\text{-}N2}$ – diffusion coefficients of oxygen in nitrogen, M is the molecular mass of the mixture, M_i is the molecular mass of i substance, other notations are the same as in (1). Water saturation pressure is calculated from the following semiempirical approximation [30]:

$$\ln p_w^{sat} = -5.80022\times10^3/T + 1.39150 - 4.86402\times10^{-2}\left(T + 4.176\times10^{-5}\right)T^2 - 1.44521\times10^{-7}\left(T^3 + 6.54597\right)\ln T \quad . \tag{4}$$

The binary diffusion coefficients are taken from Slattery and Bird estimation [31], which at low temperatures shows that they are dependent on critical temperatures $T_{c,I,j}$ pressures$p_{c,I,j}$ and masses $M_{i,j}$ of the respective components i and j, pressure of gas p, and temperature T, as represented by equation

$$pD_{i-j} = a\left(\frac{T}{\sqrt{T_{c,i}T_{c,j}}}\right)^b \left(p_{c,i}p_{c,j}\right)^{\frac{1}{3}}\left(T_{c,i}T_{c,j}\right)^{\frac{5}{12}}\left(\frac{1}{M_i}+\frac{1}{M_j}\right)^{\frac{1}{2}}, \tag{5}$$

where $a=3.640\times10^{-4}$, $b=2.334$ for water–oxygen and water–nitrogen and $a=3.64\times10^{-4}$, $b=1.823$ for oxygen–nitrogen diffusion coefficients.

With oxygen concentration varying from zero in catalyst layer to the maximum possible value in saturated humid air, the change in density-diffusivity product ρD_{O2} is negligible (less than 4%) under normal fuel cell operation conditions [18]. Then at low pressures and constant temperature the following combinations of variables are constants:

$$\alpha = pD_{O2}/RT = const,\ \beta = k/\mu RT = const\ . \tag{6}$$

The above set of equations (1) with boundary conditions (2) possesses simple analytical solution for the concentration $c_{O2}(x,y)$:

$$c_{O2}(x,y) = \cos Fx\left(E_1 \exp\frac{H-G}{2}y + E_2 \exp\frac{H+G}{2}y\right) \quad ,$$

$$E_1 = \frac{c_0 - c_1\exp\left\{-\frac{G+H}{2}d\right\}}{1-\exp\{-Gd\}},\ E_2 = \frac{-c_0\exp\{-Gd\} + c_1\exp\left\{-\frac{G+H}{2}d\right\}}{1-\exp\{-Gd\}}, \tag{7}$$

$$G = \sqrt{4F^2+H^2}\ ,\ F = \frac{\pi}{2h},\ H = -\frac{\beta}{\alpha}\frac{p_2^{\ 2}-p_1^{\ 2}}{2d}.$$

Here p_1, p_2 are the pressures in the two points of the two channels in question, d is the distance between those points, h is the thickness of the diffusive layer, c_0 – initial concentration of oxygen in "in" channel, c_1 – final concentration of oxygen in "out" channel, α and β are given by formulae (6).
The expressions (7) for the concentration yield the flux through the membrane J_{O2} as follows:

$$J_{O2} = \int_0^d j_{Ax}(h,y)dy = \alpha\frac{\pi}{h}\left(\frac{E_1}{H-G}\exp\frac{H-G}{2}y + \frac{E_2}{H+G}\exp\frac{H+G}{2}y\right). \qquad (8)$$

For the case of two parallel channels at $y=0$ and $y=d$, the oxygen flux per unit of channel length through the catalyst surface J_{O2} is at its maximum, determined by a transcendental function of the ratio $q=d/h$ of the distance between two channels to the diffuser thickness, as well as of the physical parameters ratio α/β and the difference p_1^2-p_2^2. Diffuser with permeability $k\sim10^{-7}-10^{-8}cm^2$ and $p_1=10^5Pa$, $\delta p=2\times10^3Pa$ transports oxygen to the membrane most effectively when the ratio $q\sim5-10$.

When pressure and its drop are sufficiently high, i.e., p_1^2-$p_2^2\geq2\pi q(\alpha/\beta)$, $q=d/h$, D'Arcy flow dominates over diffusion in y direction. Asymptote of catalyst oxygen flux J_{O2} at high pressures and drops, i.e., p_1^2-$p_2^2>>q^2(\alpha/\beta)$, is independent of pressure, its drop and permeability, as the diffuser is saturated with oxygen. At lower pressures, i.e., $2\pi q(\alpha/\beta)<p_1^2$-$p_2^2<q^2(\alpha/\beta)$ the flux J_{O2} is proportional to p_1^2-p_2^2, but it is independent of the diffusion coefficient. Note that the flux appears to depend on the dimensionless ratio q but not on the geometric sizes d and h. When p_1^2-$p_2^2\leq2\pi q(\alpha/\beta)$, oxygen is transported by diffusion alone.

Application of the 3-D model to the electrode of the PEFC with serpentine gas channels

In reality, the length of a gas supply channel L in PEFC is greater than the distance between them d and diffuser thickness h: L>>d, $L>>h$. Then the following relations $\partial p/\partial y >> \partial p/\partial z$, $\nabla p \| \vec{y}$ hold everywhere in interdigitated channel net, but for the vicinity of the turn points in continuous channel net. Contribution of the last is small, respectively to the rest of the net, particularly because of the low pressure drop between neighbouring channels at the turn points. Consequently, gas fluxes, directed along the supply channels in the diffuser are negligible respectively to those across the diffuser. Considering

cathode, the integration of the oxygen flux through the catalyst surface at $x=h$ over two neighbouring channels along the channel results on the following expression:

$$\Omega_{O2} = \alpha \frac{\pi}{h} \int dz \left(\frac{E_1(z)}{H(z)-G(z)} \exp \frac{H(z)-G(z)}{2} y + \frac{E_2(z)}{H(z)+G(z)} \exp \frac{H(z)+G(z)}{2} y \right), \quad (9)$$

where E_1, E_2, G, H, F are given by expressions (7), where $p_1(z)$, $c_0(z)$ are the inlet channel pressure and oxygen concentration, $p_2(z)$, $c_1(z)$ are the outlet channel pressure and oxygen concentration respectively, α and β are constants, given by formulae (6), d is the distance between the channels.

Expression (9), applied to the plate of serpentine channels, yields the total flux through the membrane plane in the following form:

$$\Omega_{serp} = \pi\alpha \frac{L}{h} \sum_{i=1}^{n-1} \left(\frac{E_{1i}}{H_i - G_i} \exp \frac{H_i - G_i}{2} y + \frac{E_{2i}}{H_i + G_i} \exp \frac{H_i + G_i}{2} y \right), \quad (10)$$

$$E_{1i} = \frac{c_{0i} - c_{1i} \exp\left\{ -\frac{G_i + H_i}{2} d \right\}}{1 - \exp\{-G_i d\}}, \quad E_{2i} = \frac{-c_{0i} \exp\{-G_i d\} + c_{1i} \exp\left\{ -\frac{G_i + H_i}{2} d \right\}}{1 - \exp\{-G_i d\}}, \quad (11)$$

$$G_i = \sqrt{4F^2 + H_i^2}, \quad F = \frac{\pi}{2h}, \quad H_i = -\frac{\beta}{\alpha} \frac{p_{2i}^2 - p_{1i}^2}{2d},$$

where E_1, E_2, G, H, F are given by formulae (7), α, β are given by formulae (6), $d=W/(n-1)$, n is the number of channels, W is the width of the channel plate, L is the length of *one section* of the serpentine channel, p_{1i}, p_{2i}, c_{0i} c_{1i} are average values of proper variables in every channel, and other notations are the same as in formulae (7).

In view of rather small pressure and concentration drops, linearisation can be performed as follows:

$$p_{1i} = p_{in} + (i - 1/2)\delta p, \quad \delta p = \frac{p_{out} - p_{in}}{n-1}, \quad d = \frac{W}{(n-1)}, \quad (12)$$

$$c_{0i} = c_{0\,in} + (i - 1/2)\delta c_0,\ \delta c_0 = \frac{c_{0\,out} - c_{0\,in}}{n-1},\ c_{1i} = c_{0i} - \delta c_0,$$

where p_{out} is the outlet gas pressure, p_{in} is the inlet gas pressure, c_{0out} is the outlet reactant concentration, c_{0in} is the inlet reactant concentration, n is the number of supply channels, h is the thickness of the diffusive layer, d is the distance between the neighbouring channels, W is the width of the channel plate.

Current limitations in PEFC with 2, 3, 4, 5, 7 and 10 gas supply channels in serpentine

1. Non flooded model

In this section, the above described model of the gas transport in porous diffuser of the electrode of PEFC is applied for the comparative analysis of the maximum current limitations of the PEFC for several specific configurations of gas supply channels, represented serpentine design. The comparison is hold between nets of 2, 3, 4, 5, 7 and 10 parallel channels machined in serpentine on a square plate. The aim of the studies is the identification of most efficient in the terms of the limiting current, channel configuration.

Reduce the variety of possible serpentine configurations to that, schematically given on Fig.4, with the effective average pressures in channels derived from the approximation of linear pressure drop.

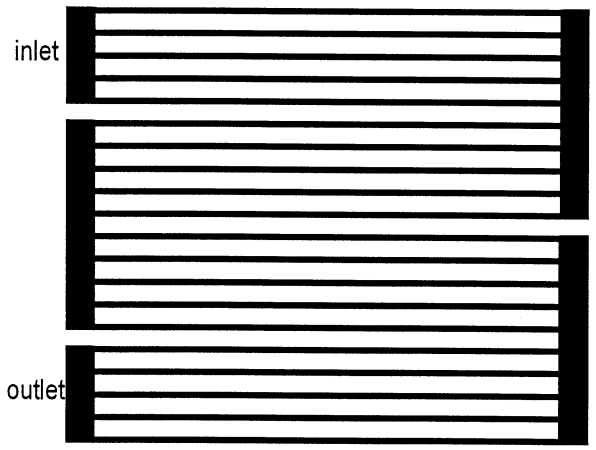

SERPENTINE design; MxN channels.

Channel structure on the plate: N sections x M channels.
25x2, 17x3, 13x4, 10x5, 7x7, 5x10 channels.

Geometric parameters of the modelled device:

width of each channel r= approximately 1mm,
distance between the channels d= approximately 1mm,
channel section length L=100mm,
total plate width 100mm,
effective diffussion length h=0.25mm.

Figure 4. *Schematic illustration of serpentine configuration of n parallel gas channels in a PEFC.*

The limiting current of the PEFC is determined by the maximum oxygen flow, converted on the catalyst. Suppose that the electrochemical processes are equal for both configurations, additional losses in the catalyst layer and those, coming due to ohmic resistance are equal for all channel configurations. We also neglect the effect of flooding of the diffuser by liquid water on this stage. Set equal pressure regime for both configurations of channels. The developed model, applied for the studies of air flows through the diffuser of PEFC over two, three and ten serpentine gas supply channels under equal pressures predicts higher values of the maximum O_2 catalyst flux for smaller number of channels in section.

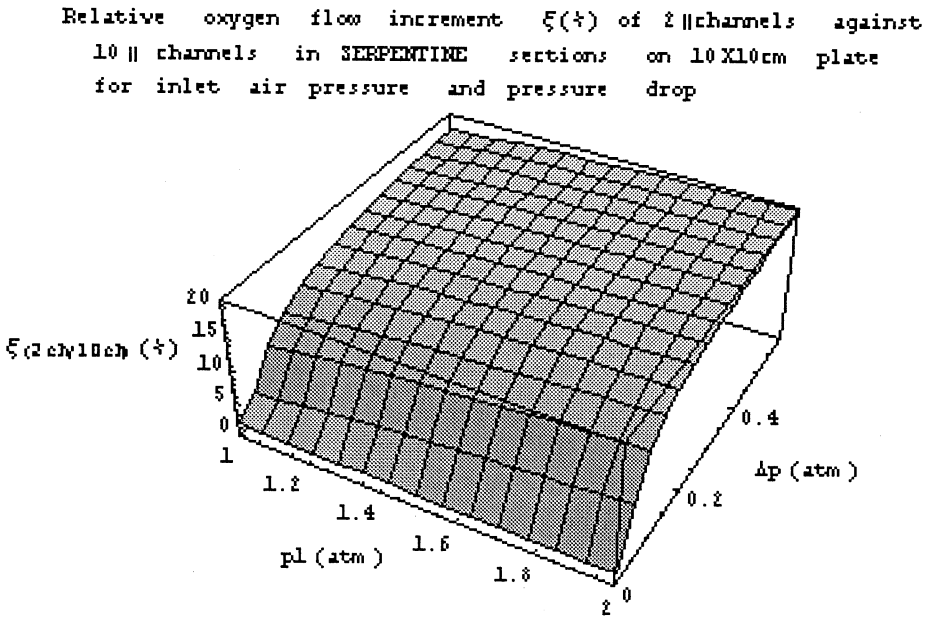

Figure 5. *Relative increment of the maximum oxygen flow in diffuser over 2 channel serpentine, respectively to 10-channel serpentine for inlet pressure p_1 and pressure drop Δp.*

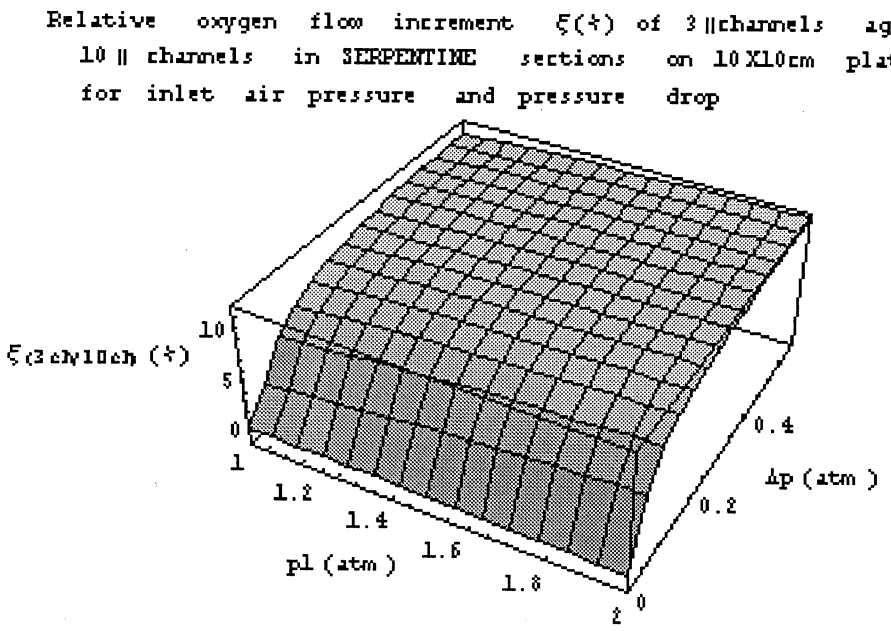

Figure 6. *Relative increment of the maximum oxygen flow in diffuser over 3 channel serpentine, respectively to 10-channel serpentine for inlet pressure p_1 and pressure drop Δp.*

The Fig.s 5 and 6 demonstrate up to *15–20%* increase of the maximum oxygen flow through the catalyst, for three and, particularly, for two channel serpentine, respectively to ten channel net. Consequently, we expect the same value for the relative increase of the limiting current of the cell.

However, more realistic situation can be modelled in the following way. Fix the inlet pressure, and vary the oxygen flow in the gas supply channel, following the electric current of the cell. Then, Δp will be specific for each channel configuration, i.e. 2, 3, etc. channels in a serpentine section, for the same current. This predictions of the model, based on the evaluation for the airflow values approximately equal to *40 $cm^3/min/A$* result in 13% limiting oxygen flux increase for 3 channel serpentine, respectively to 10-channel design.

The predicted values of the relative increment of the limiting current (due to oxygen transport) for various numbers of channels in serpentine are given in the Table 1.

M x N channels x sections	10x5 (P_1=1.6atm)	7x7 (P_1=1.6atm)	5x10 (P_1=1.6atm)	4x13 (P_1=1.7atm)	3x17 (P_1=1.7atm)	2x25 (P_1=1.75atm)
Maximum current $I_{M\,ch}$ to I_{10ch} (%)	**0%**	**3%**	**6%**	**9%**	**13%**	**21%**
Pressure drop $\Delta P=P_{in}-P_{out}$ (atm)	**0.05**	**0.1**	**0.2**	**0.33**	**0.57**	**1.25**

Table 1. *Relative increment of the limiting current, coming due to oxygen transport limitations in M channel serpentine, respectively to 10 channel serpentine for equal air flow to electric current ratio.*

2. Flooded model

In order to take into account the presence of liquid water in the porous of the gas diffuser, the effective porosity will be introduced now. It describes the porous media when the porous are partially filled with liquid water in thermodynamic and hydrodynamic equilibrium. The quantity of liquid water, retained by gas diffuser, depends on the nature of the mass transport in it. Due to the pressure gradient between the neighbouring serpentine sections, forced convection helps removing the majority of water from the diffuser there. Where the gas channel lies, a certain part of the liquid water is removed from the diffuser just over it due to the channel gas flow. The diffuser over the shoulders between the channels within a section of the serpentine is probable to be mostly flooded, since the water does not have an immediate exit to the gas channel and neither the convection contributes to its removal due to the absence of the pressure drop between such channels. Although, it is hard to measure and obtain precise information about the quantities of liquid water in various points of the diffuser, we suppose that the water reduces the volume of the porous in the diffuser by maximum a quarter, whereas the removal of the water by convection is complete.

Consider the following flooded model, where 12% of porous in the diffuser over the channels and 25% or porous in the diffuser between the channels of each serpentine section are flooded by liquid water. Then the porosity in each domain is equal to $\varepsilon_1=0.8$, $\varepsilon_2=0.7$, $\varepsilon_3=0.6$ respectively. Account for the effective tortuosity and porosity of the diffuser will be carried out through the Bruggeman–type correction, which estimates effective oxygen diffusion coefficient with the following relation:

$$D_{O2}{}^{eff}{}_{i} = D_{O2}\varepsilon_i{}^{\tau}, \tag{13}$$

where D_{O2} is determined by formula (3), ε_i and τ are porosity and tortuosity factors of the diffuser in i domain. Three different domains of the diffuser are those over the channel, between the channels within a section and between the sections of the serpentine. The above discussed modelling of the diffuser with the number of channels in serpentine varying from 2 to 10 results in the following predictions of the oxygen transport limitations of the cell for two pressure regimes, given in the Tables 2 and 3:

M channels x N sections	10x5 (P_1=1.6atm)	7x7 (P_1=1.6atm)	5x10 (P_1=1.6atm)	4x13 (P_1=1.7atm)	3x17 (P_1=1.7atm)
Maximum current $I_{M\,ch}$ to I_{10ch} (%)	**0%**	**4%**	**10%**	**15%**	**24%**
Pressure drop $\Delta P=P_{in}-P_{out}$ (atm)	0.075	0.14	0.27	0.46	0.85

Table 2. *Relative increment of the limiting current, coming due to oxygen transport limitations* ***in partially flooded model*** *in M channel serpentine, respectively to 10 channel serpentine for constant air flow to electric current ratio for ΔP=0.075atm for 10 channel geometry.*

M channels x N sections	10x5 (P_1=1.6atm)	7x7 (P_1=1.6atm)	5x10 (P_1=1.6atm)	4x13 (P_1=1.7atm)	3x17 (P_1=1.7atm)	2x25 (P_1=1.7atm)
Maximum current $I_{M\,ch}$ to I_{10ch} (%)	**0%**	**4%**	**9%**	**15%**	**23%**	**39%**
Pressure drop $\Delta P=P_{in}-P_{out}$ (atm)	0.035	0.06	0.13	0.21	0.4	0.9

Table 3. *Relative increment of the limiting current, coming due to oxygen transport limitations* ***in partially flooded model*** *in M channel serpentine, respectively to 10 channel serpentine for constant air flow to electric current ratio for ΔP=0.035atm for 10 channel geometry.*

Comparing Tables 2 and 1 we note that with the account for the liquid water, present in the porous, the efficiency of the serpentine with low number of channels in sections becomes even more evident. The limiting oxygen flow increase for $M=3$ channels in serpentine now equals to $22–25\,\%$ against $13\,\%$ predicted with no account for water flooding. The pressure regime is chosen so that the airflow in the channels is independent on the channel configuration; for example, the values in table 3 and 5 are calculated for the airflow $\approx 50\ cm^3/min/A$. Variations in the air flow and consequently in the pressure regime, reported in Tables 2 and 3 effects the predictions for the maximum catalyst oxygen flux only slightly. However, it may be difficult to maintain sufficient air supply, independent on different channel sets, because the required pressure drop should be high for low number of channels in a section M.

Besides the above described modelling of the electrode flooding, the dynamic model of the flooding effect in the electrode is developed. It is presumed that the percentage of the porous, available for gas transport depends on the pressure gradient ∇p exponentially, so the effective porosity varies from $\varepsilon_l=0.8$ when all the water is removed by the shear flow with $\nabla p \geq 0.2 atm/cm$ pressure gradient, to $\varepsilon_l=0.55$ when $\nabla p=0$. Such approach results in the following predictions, given in the Tables 4 and 5:

M channels x N sections	10x5 (P_1=1.6atm)	7x7 (P_1=1.6atm)	5x10 (P_1=1.6atm)	4x13 (P_1=1.7atm)	3x17 (P_1=1.7atm)
Maximum current $I_{M\,ch}$ to I_{10ch} (%)	**0%**	**4%**	**10%**	**16%**	**25%**
Pressure drop $\Delta P=P_{in}-P_{out}$ (atm)	0.075	0.14	0.27	0.46	0.85

Table 4. *Relative increment of the limiting current, coming due to oxygen transport limitations* ***in dynamical flooded model*** *in M channel serpentine, respectively to 10 channel serpentine for constant air flow to electric current ratio for $\Delta P=0.075atm$ for 10 channel geometry.*

M channels x N sections	10x5 (P_1=1.6atm)	7x7 (P_1=1.6atm)	5x10 (P_1=1.6atm)	4x13 (P_1=1.7atm)	3x17 (P_1=1.7atm)	2x25 (P_1=1.7atm)
Maximum current $I_{M\,ch}$ to I_{10ch} (%)	**0%**	**3%**	**8%**	**13%**	**22%**	**40%**
Pressure drop $\Delta P=P_{in}-P_{out}$ (atm)	0.035	0.06	0.13	0.21	0.4	0.9

Table 5. *Relative increment of the limiting current, coming due to oxygen transport limitations* ***in dynamical flooded model*** *in M channel serpentine, respectively to 10 channel serpentine for constant air flow to electric current ratio for ΔP=0.035atm for 10 channel geometry.*

The predictions of dynamical and partially flooded models appear to be similar, as the comparison of the Table 2 with the Table 4 and Tables 3, 5 evidences. For low pressure drops, dynamic flood model predicts slightly lower performance of 7, 5 and 4 channel serpentines respectively to the predictions of the partially flooded model – 3%, 8% and 13% against 4%, 9% and 14% increase (see tables 3 and 5), compared with 10 channel serpentine. At higher pressure drops the dynamic model shows slightly higher results – 16% for M=4 and 25% for M=3, against 15% and 24% respectively for 4 and 3 channels in partially flooded model (See Tables 2 and 4, also compare the results for M=2 in the Tables 3 and 5).

Discussion and conclusions

The experimental measurements, demonstrated $\approx 25\%$ higher cell current for *3*-channel parallel serpentine against *10*-channel configuration in the high current regime, when the air flow in air supply channels followed the produced electric current at $52 cm^3/min/A$ (The maximum current was limited at 0.6 A/cm^2 due to technical reasons). This experimental data are in agreement with predicted theoretical values and demonstrate the same tendency, i.e. the efficiency of the PEFC at high currents increases with the decrease of the number of supply channels in a serpentine section M with independently constant air flux in supply channels. However, it requires high pressure drops Δp for serpentines with $M=2$ and $M=3$. Developed with no account for liquid water model predicts 13% current increase for *3*-channel net

respectively to 10-channel net (See Table 1). It agrees with the experiment only qualitatively. The difference between experimental and model values can be explained by the effect of liquid water, present on the cathode side in the porous diffuser, but very difficult to model. Due to the big number of sections and higher Δp between the sections (which is necessary to provide fixed air supply) in $M=2$ and $M=3$, respectively to $M=10$ channel serpentines, the air is forced to flow in the diffuser between the channels of neighbouring sections. This effect helps removing the liquid water from the porous, since molecular diffusion becomes combined with forced convection in the matter.

Really, developed with the account for the liquid water models predict $22–25\%$ higher performance of 3 channel serpentine, respectively to 10 channel serpentine in the terms of the limiting current. These values are in agreement with experimental measurements. The predictions of dynamical and partially flooded models appear to be similar, as we can see that from the comparison of Tables 2 and 3 with Tables 4 and 5 respectively. Dynamic flood modelling yields some weaker advantage for of 7, 5 and 4 channel serpentines than partially flooded model does at low pressure drops (see Tables 3 and 5).

However, the higher the pressure, the better the liquid water is removed from the pores and the higher the predictions of the dynamic model become. It also predicts higher limiting currents than it is expected with constant flooding (see Tables 2 and 4 for M=4 and M=3, also see the results for M=2 in the Tables 3 and 5). Although the difference between the predictions in Tables 4 and 5 is about of 2-3% for 3, 4 and 5 channels, this important dependence on the pressure regime, accounted for in the dynamical model, is in agreement with few available experimental observations, which demonstrate that the limiting current generally increases slightly with the rise of the pressure and its drop.

The agreement between theoretical predictions of the developed model and the data of experimental measurements indicates on the correct account for the complex of the physical phenomena, responsible for the differences in current limits between geometric configurations and its adequate modelling.

It is important to underline that maximum current increase for 2 channel net I_{2ch}/I_{10ch} could reach 35-40%, but to obtain equal air supply flux for M=10 and M=2 channel geometry, the pressure drop in the last case should be $\Delta P_{2channel\ net} \sim 1.8atm$ if $\Delta P_{10channel\ net} \sim 0.075atm$ and $\Delta P_{2channel\ net} \sim 0.85atm$ if $\Delta P_{10channel\ net} \sim 0.035atm$, requiring high inlet pressure. Due to technical reasons, such a regime was impossible and the inlet pressure was fixed at $\approx 1.6atm$.

The results obtained and discussed above lead to the following general conclusions:

- Due to the forced convection mechanism, serpentine gas supply channel nets with small number of channels M in each section provide higher limits on directed to catalyst O_2 flux in diffuser and therefore higher limits on the maximum current. Gas supply configurations with two and three channels were identified as the best for the high limiting current. (Dependently on the pressure regime,

up to 25% increase for 3 channel net and up to 35-40% increase for 2 channel respectively to the serpentine of M=10 channels in a section).

- Negative effect of water flooding in diffuser is reduced when serpentines with low M channels in a section and high number of sections N are employed.
- Very small number of channels (M=1, 2) in a serpentine section may result in significant deplete of oxygen along the channels due to insufficient air supply at low pressure drops and require high pressure drops.

Modelling oxygen transport in the diffuser of the PEFC with pressure $1atm<P<2atm$, $0atm<\Delta P<0.5atm$ and the number of channels in each serpentine section M=2, 3, …, 10, we conclude that serpentine channel nets with M=3 and M=2 channels in each section provide higher limits on catalyst oxygen flux in diffuser and therefore establish higher limits on the maximum current: up to 13% more for N=3 and 20% increase for N=2, respectively to M=10 channels in serpentine. (See Fig.s 5 and 6).

Modelling oxygen transport in the diffuser of the PEFC with liquid water flooding at the air flow ~50scc/min/A, and the number of channels in a section M=2, 3, …, 10, we found the predictions of the model in agreement with experimental data.

- With the account for flooding of the diffuser by liquid water, serpentines with M= 4, 3 or 2 channels in a section appear to be more effective than 10 channel design, providing even higher limits onthe maximum current that the model without flooding: up to 25% for M=3 (See Tables 2, 4). Serpentine with M=2 would provide 35-40% higher current limits that M=10 channel net (See Tables 3, 5), but it would also require high pressure drops to maintain required air flux.
- Dynamic modelling of flooding, accounting for liquid water removal by shear gas flow in diffuser, dependent on the pressure gradient, predicts few percent better performance of the PEFC working with higher pressure and pressure drop. This agrees with experimental observations.

The effect of flooding of the electrode can be investigated deeper in future studies together with further adjustments of the model. Additional experimental tests are foreseen.

Acknowledgements

Thanks are due to Ing. M.Brocco and Ing. M.Pasquali for fruitful conversations and discussions.

References:

1. M.S.Wilson and S.Gottesfeld, "High performance catalysed membranes of ultralow Pt loadings for PEFC" *J. Electrochem. Soc.* **139**, L28 (1992).
2. E.J.Taylor, E.B.Anderson and N.R.K.Vilambi, "Preparation of High-Platimun-Utilization gas Diffusion Electrodes for PEM Fuel Cells", *J. Electrochem. Soc.* **139**, L45 (1992).
3. G.S.Kumar, M.Raja and S.Parthasarathy, "High Performance Electrodes with very low Platinum Loading for Polymer Electrolyte Fuel Cells ", *Electrochim. Acta* **40**, 285 (1995).
4. T.R.Ralph, G.A.Hards, J.E.Keating, S.A.Campbell, D.P.Wilkinson, M.Davis, J.St-Pierre and M.C.Johnson, "Low Cost Electrodes for PEM Fuel Cells", *J. Electrochem. Soc.* **144**, 3845 (1997).
5. T.V.Nguyen and R.E.White, "A Water and Heat Management Model for PEM Fuel Cell", *J.Electrochem. Soc.* **140**, 2178 (1993).
6. T.E.Springer, T.A. Zawodzinski, M.S. Wilson, S. Gottesfeld, "Characterization of Polymer Electrolyte Fuel Cells Using AC Impedance Spectroscopy", *J. Electrochem. Soc.* **143**, N2, 587 (1996).
7. T. Toda, H. Igarashi, M. Watanabe "Role of Electronic Property of Pt and Pt Alloys on Electrocatalytic Reduction of Oxygen" *J. Electrochem. Soc.* **145**, 12, 4185 (1998).
8. J.S.Wainright, J.-T.Wang, D.Weng, R.F.Savinell and M.Litt, "Acid Doped Polibenzimidazoles: A new Polymer Electrolyte", *J. Electrochem. Soc.* **142**, L121 (1995).
9. M.Watanabe, Y.Satoh, C.Shimura, "Management of Water Content in Polymer Electrolyte Membranes with Porous Fiber Wicks" , *J. Electrochem. Soc.* **140**, N11, 3190 (1993).
10. T.E.Springer, T.A.Zawodzinski and S.Gottesfeld, "Polymer Electrolyte Fuel Cell Model", *J.Electrochem. Soc.* **138**, 2334 (1991).
11. M.L.Perry, J.Newman, E.J.Cairns. "Mass Transport in Gas-Diffusion Electrodes: A Diagnostic Tool for Fuel-Cell Cathodes", *J. Electrochem. Soc.* **145**, N1, 5 (1998).
12. D.M.Bernardi and M.W.Verbrugge. "Mathematical Model of a Gas Diffusion Electrode Bonded to a Polymer Electrolyte", *AIChE Journal*, **37**, No8, 1151 (1991).
13. D.M.Bernardi and M.W.Verbrugge. "A Mathematical Model of the Solid Polymer Electrolyte Fuel Cell", *J. Electrochem. Soc.* **139**, N9, 2477 (1992).
14. Y.W.Rho, S.Srinivasan, Y.T.Kho, "Mass Transport Phenomena in Proton Exchange Membrane Fuel Cells Using O_2/He, O_2/Ar, and O_2/N_2 Mixtures", *J. Electrochem. Soc.* **141**, N8, 2089 (1998).
15. D.M.Bernardi, "Water Balance Calculations for Solid-Polymer-Electrolyte Fuel Cells", *J. Electrochem. Soc.* **137**, N11, 3344 (1990).
16. T.F.Fuller, J.Newman, "Water and Thermal management in Solid-Polymer-Electrolyte Fuel Cells", *J. Electrochem. Soc.* **140**, N5, 1218 (1993).
17. J.C.Amphlett, R.M.Baumert, R.F.Mann, B.A.Peppley, P.R.Roberge and T.J.Harris, "Performance modelling of the Ballard Mark IV Solid Polymer Electrolyte Fuel Cell", *J. Electrochem. Soc.* **142**, N1, 1 (1995).

18. V.Gurau, F. Barbir, H. Liu. "An Analytical solution of a Half-Cell Model for PEM Fuel Cells". *J. Electrochem. Soc.* **147**, N7, 2468 (2000).
19. W.He, J.S.Yi, T.V.Nguyen, "Two-Phase Flow Model of the Cathode of PEM Fuel Cells Using Interdigitated Flow Fields", *AIChE Journal*, **46**, No.10, 2053 (2000).
20. T.V.Nguyen, " A Gas Distribution Design for PEM Fuel Cells", *J.Electrochem Soc.* **143**, L103 (1996).
21. J.S.Yi and T.V.Nguyen, "An Along the Channel Model for Proton Exchange Membrane Fuel Cells", *J. Electrochem. Soc.* **145**, 1149 (1998).
22. A. Pozio, L. Giorgi, M. De Francesco, R.F. Silva, R. Lo Presti, A. Danzi, "Membrane electrode gasket assembly (MEGA) technology for polymer electrolyte fuel cells", *J. Power Sources*, **112**/2 (2002) 491.
23. L. Giorgi, E. Antolini, A. Pozio, E. Passalacqua, "Influence of the PTFE content in the diffusion layer of low-Pt loading electrodes for polymer electrolyte fuel cells". *Electrochim. Acta* **43** (1998) 3675.
24. A. Pozio, L. Giorgi, E. Antolini, E. Passalacqua, 'Electroxidation of H_2 on Pt/C Pt–Ru/C and Pt–Mo/C anodes for polymer electrolyte fuel cell", *Electrochim. Acta* **46** (2000) 555.
25. J.Newman and W.Tiedemann, "Porous-Electrode Theory with Battery Applications",*AIChE Journal.*, **21**, 25 (1975).
26. K.R.Weisbrod, S.A.Grot and N.E.Vanderborgh, in Proton Conducting Membrane Fuel Cells I, S.Gottesfeld, G.Halpert and A.Landgrebe, Editors, PV 95-23, p.152, The Electrochemical Society Proceedings Series, Pennington, NJ (1998).
27. T.E.Springer and S.Gottesfeld, in Modelling of batteries and Fuel Cells, R.E.White, M.W.Verbrugge and J.F.Stockel, Editors, PV 91-10, p.197, The Electrochemical Society Proceedings Series, Pennington, NJ (1991).
28. M.Eikerling and A.A.Kornyshev, "Modelling the performance of the cathode catalyst layer of polymer electrolyte fuel cells", *J.Electroanal. Chem.*, **453**, 89 (1998).
29. F.M.White, *Viscous Fluid Flow*, NY:Mc.Draw Hill, New York (1991).
30. *ASHRAE Handbook, Fundamentals*, American Society of Heating, Refrigerating and Air Conditioning Engineers, Inc. (1981)
31. R.B.Bird, W.E.Steward and E.N.Lighfoot, *Transport phenomena*, John Willey & Sons, New York (1960).

List of Figure Captions

Figure 1. Schematic of a single PEM fuel cell showing the location of the components: A) aluminium or SS316L end plates, B) copper current collector/gaskets, C) graphite flow field plates, D) MEGA

Figure 2. Cell voltage and power density vs. current density for 3 (squares) and 10 (circles) cathode channels configuration, at T_{cell}=75°C under H_2 14 scc/min/A and O_2 52.5 scc/min/A flux at 1.5/1.5 abs bar.

Figure 3. Schematic drawing of an electrode of a polymer electrolyte fuel cell.

Figure 4. Schematic illustration of serpentine configuration of n parallel gas channels in a PEFC.

Figure 5. Relative increment of the maximum oxygen flow in diffuser over 2 channel serpentines, respectively to 10-channel serpentine for inlet pressure p_1 and pressure drop Δp.

Figure 6. Relative increment of the maximum oxygen flow in diffuser over 3 channel serpentines, respectively to 10-channel serpentine for inlet pressure p_1 and pressure drop Δp

List of Table Captions

Table 1. Relative increment of the limiting current, coming due to oxygen transport limitations in M channel serpentine, respectively to 10 channel serpentine for equal air flow to electric current ratio.

Table 2. Relative increment of the limiting current, coming due to oxygen transport limitations **in partially flooded model** in M channel serpentine, respectively to 10 channel serpentine for constant air flow to electric current ratio for ΔP=0.075atm for 10 channel geometry.

Table 3. Relative increment of the limiting current, coming due to oxygen transport limitations **in partially flooded model** in M channel serpentine, respectively to 10 channel serpentine for constant air flow to electric current ratio for ΔP=0.035atm for 10 channel geometry.

Table 4. Relative increment of the limiting current, coming due to oxygen transport limitations **in dynamical flooded model** in M channel serpentine, respectively to 10 channel serpentine for constant air flow to electric current ratio for ΔP=0.075atm for 10 channel geometry.

Table 5. Relative increment of the limiting current, coming due to oxygen transport limitations **in dynamical flooded model** in M channel serpentine, respectively to 10 channel serpentine for constant air flow to electric current ratio for ΔP=0.035atm for 10 channel geometry.

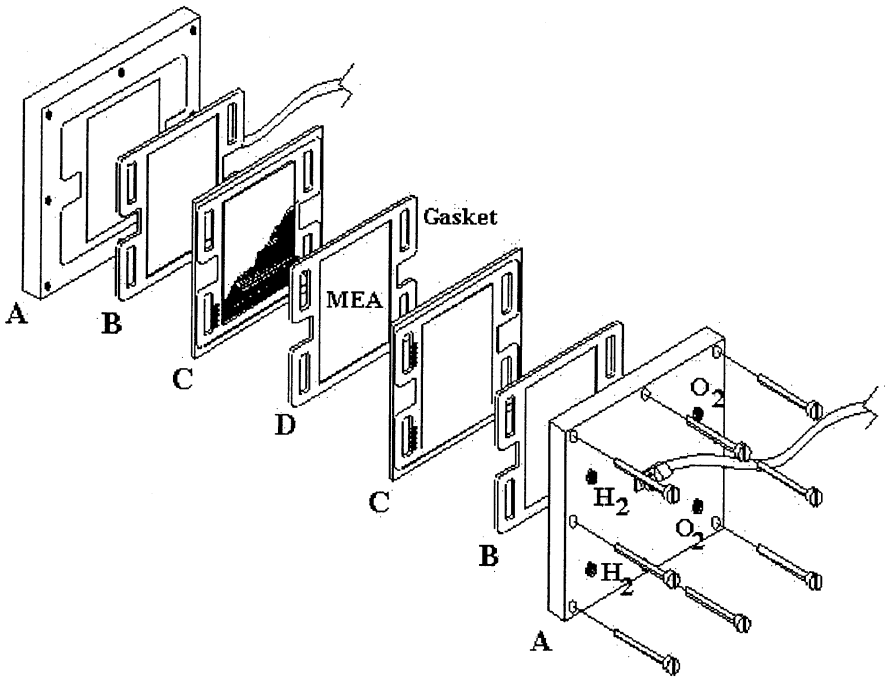

Figure 1. *Schematic of a single PEM fuel cell showing the location of the components: A) aluminium or SS316L end plates, B) copper current collector/gaskets, C) graphite flow field plates, D) MEGA*

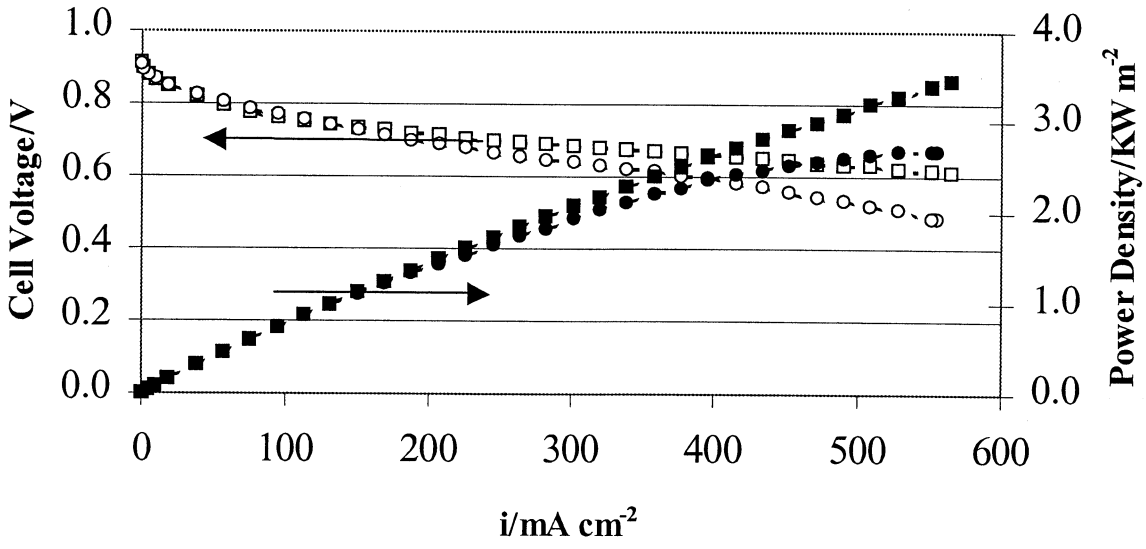

Figure 2. *Cell voltage and power density vs. current density for 3 (squares) and 10 (circles) cathode channels configuration, at T_{cell}=75°C under H_2 14 scc/min/A and O_2 52.5 scc/min/A flux at 1.5/1.5 abs bar.*

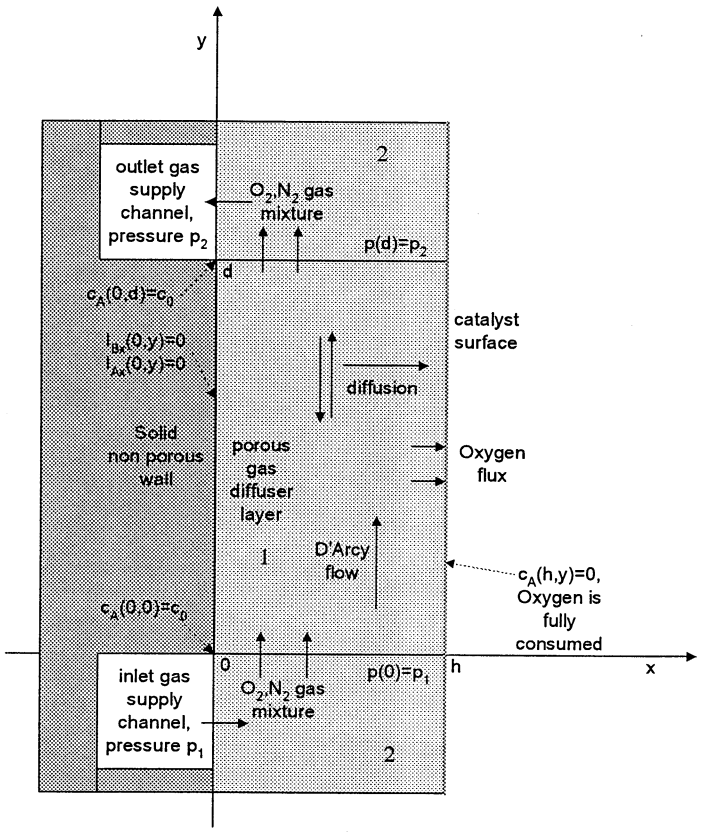

Figure 3. *Schematic drawing of an electrode of a polymer electrolyte fuel cell.*

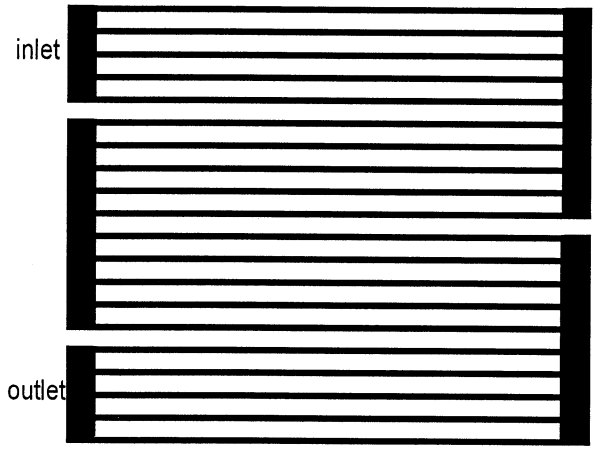

SERPENTINE design; MxN channels.

Channel structure on the plate: N sections x M channels.
25x2, 17x3, 13x4, 10x5, 7x7, 5x10 channels.

Geometric parameters of the modelled device:

width of each channel r= approximately 1mm,
distance between the channels d= approximately 1mm,
channel section length L=100mm,
total plate width 100mm,
effective diffussion length h=0.25mm.

Figure 4. *Schematic illustration of $n=MxN$ parallel channels serpentine configuration of gas supply channels in a PEFC.*

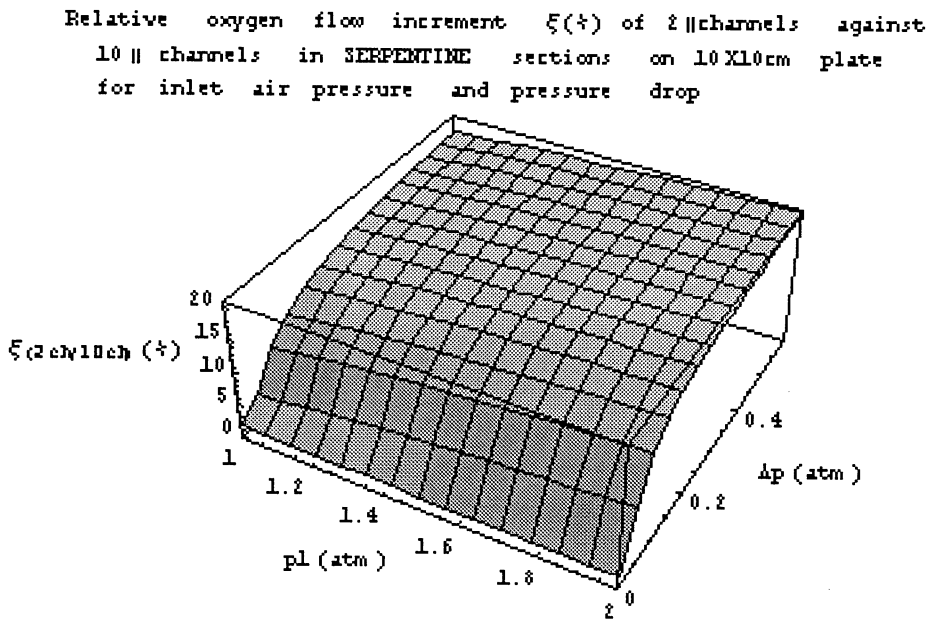

Figure 5. *Relative increment of the maximum oxygen flow in diffuser over 2-channel serpentine, respectively to 10-channel serpentine for inlet pressure p_1 and pressure drop Δp.*

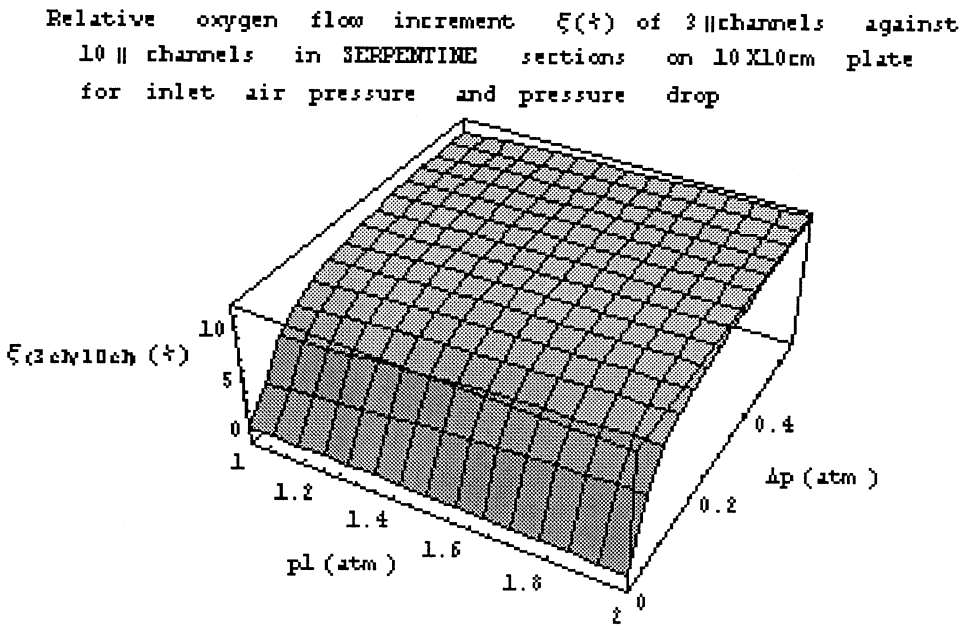

Figure 6. *Relative increment of the maximum oxygen flow in diffuser over 3-channel serpentine, respectively to 10-channel serpentine for inlet pressure* p_1 *and pressure drop* Δp.

M x N channels x sections	10x5 (P_1=1.6atm)	7x7 (P_1=1.6atm)	5x10 (P_1=1.6atm)	4x13 (P_1=1.7atm)	3x17 (P_1=1.7atm)	2x25 (P_1=1.75atm)
Maximum current $I_{M\,ch}$ to I_{10ch} (%)	**0%**	**3%**	**6%**	**9%**	**13%**	**21%**
Pressure drop $\Delta P=P_{in}-P_{out}$ (atm)	**0.05**	**0.1**	**0.2**	**0.33**	**0.57**	**1.25**

Table 1. *Relative increment of the limiting current, coming due to oxygen transport limitations in M channel serpentine, respectively to 10 channel serpentine for equal air flow to electric current ratio.*

M channels x N sections	10x5 (P_1=1.6atm)	7x7 (P_1=1.6atm)	5x10 (P_1=1.6atm)	4x13 (P_1=1.7atm)	3x17 (P_1=1.7atm)
Maximum current $I_{M\,ch}$ to I_{10ch} (%)	**0%**	**4%**	**10%**	**15%**	**24%**
Pressure drop $\Delta P=P_{in}-P_{out}$ (atm)	0.075	0.14	0.27	0.46	0.85

Table 2. *Relative increment of the limiting current, coming due to oxygen transport limitations* ***in partially flooded model*** *in M channel serpentine, respectively to 10 channel serpentine for constant air flow to electric current ratio for ΔP=0.075atm for 10 channel geometry.*

M channels x N sections	10x5 (P_1=1.6atm)	7x7 (P_1=1.6atm)	5x10 (P_1=1.6atm)	4x13 (P_1=1.7atm)	3x17 (P_1=1.7atm)	2x25 (P_1=1.7atm)
Maximum current $I_{M\,ch}$ to I_{10ch} (%)	**0%**	**4%**	**9%**	**15%**	**23%**	**39%**
Pressure drop $\Delta P=P_{in}-P_{out}$ (atm)	0.035	0.06	0.13	0.21	0.4	0.9

Table 3. *Relative increment of the limiting current, coming due to oxygen transport limitations* ***in partially flooded model*** *in M channel serpentine, respectively to 10 channel serpentine for constant air flow to electric current ratio for ΔP=0.035atm for 10 channel geometry.*

M channels x N sections	10x5 (P_1=1.6atm)	7x7 (P_1=1.6atm)	5x10 (P_1=1.6atm)	4x13 (P_1=1.7atm)	3x17 (P_1=1.7atm)
Maximum current $I_{M\,ch}$ to I_{10ch} (%)	**0%**	**4%**	**10%**	**16%**	**25%**
Pressure drop $\Delta P=P_{in}-P_{out}$ (atm)	0.075	0.14	0.27	0.46	0.85

Table 4. *Relative increment of the limiting current, coming due to oxygen transport limitations* ***in dynamical flooded model*** *in M channel serpentine, respectively to 10 channel serpentine for constant air flow to electric current ratio for ΔP=0.075atm for 10 channel geometry.*

M channels x N sections	10x5 (P_1=1.6atm)	7x7 (P_1=1.6atm)	5x10 (P_1=1.6atm)	4x13 (P_1=1.7atm)	3x17 (P_1=1.7atm)	2x25 (P_1=1.7atm)
Maximum current $I_{M\,ch}$ to I_{10ch} (%)	**0%**	**3%**	**8%**	**13%**	**22%**	**40%**
Pressure drop $\Delta P=P_{in}-P_{out}$ (atm)	0.035	0.06	0.13	0.21	0.4	0.9

Table 5. *Relative increment of the limiting current, coming due to oxygen transport limitations* ***in dynamical flooded model*** *in M channel serpentine, respectively to 10 channel serpentine for constant air flow to electric current ratio for ΔP=0.035atm for 10 channel geometry.*

Edito dall' ENEA
Funzione Centrale Relazioni Esterne
Unità Comunicazione
Lungotevere Thaon di Revel, 76 - 00196 Roma
www.enea.it
Stampa: Laboratorio Tecnografico ENEA - CR Frascati
Finito di stampare nel mese di ottobre 2003